19th Australasian Fluid Mechanics Conference
Melbourne, Australia
8-11 December 2014

Computational Investigation of Ventilated Cavity Flow Over a 2-D Fence

L. Barbaca, B.W. Pearce and P.A. Brandner

Australian Maritime College
University of Tasmania, Launceston, Tasmania 7250, Australia

Abstract

Ventilated supercavitating flow over a 2-D wall mounted fence is numerically investigated using a viscous approach. Flow was simulated using an implicit unsteady compressible solver with a RANS *k*-ω SST turbulence model and VOF approach for cavity interface tracking. All simulations were carried out for a fixed fence height based Reynolds number of 50,000. The effect of ventilation rate on the flow characteristics is investigated. The effects of the wall boundary layer were examined by comparing results with inviscid potential flow from a boundary element method. The relationship between ventilation rate and the lift and drag resulting from the respective wall and fence pressure distributions is determined. It was found that, lift increases and drag decreases with increasing ventilation rate thus increasing hydrodynamic efficiency. These numerical results will be compared with future experimental investigations to be performed in a cavitation tunnel.

Introduction

A ventilated supercavity is a gaseous cavity formed when incondensable gas is introduced into the low pressure region of a liquid flow. There are several marine applications where use of this phenomenon can lead to the significant performance improvements. The most extensively investigated application of ventilated supercavitation is its use on the axisymmetric underwater projectiles as a method to achieve drag reduction. Drag is reduced due to the formation of a gaseous bubble surrounding the body, limiting its contact with liquid, thus largely reducing skin friction. A summary of knowledge is presented by Semenenko [13]. A similar method for drag reduction is used for an application referred to as air-lubrication of the wetted part of the ship hull. Drag reduction is achieved by injecting air through specially designed devices on the ship hull bottom. This creates a partial air-ventilated cavity under the ship hull, significantly reducing friction resistance [3, 8].

Ventilation can be used on base-ventilated hydrofoils to create a stable supercavity under the conditions where a natural supercavity, i.e. from vapour alone, will not form. This enables drag reduction for foils designed to operate in the natural supercavitating regime, well before conditions required for natural supercavitation to occur are reached. Also, a novel concept of an intercepted base-ventilated hydrofoil for the ride control of a high-speed vessel is proposed by Elms [5]. In the present study some basic aspects of air-ventilated cavity flow over a wall mounted fence are investigated. Separated flow over a fence protruding from the wall has been extensively investigated within the field of aerodynamics. A fence fitted to the trailing edge of an aerofoil, also known as a Gurney flap, is used as a lift enhancement device [14] in aerospace and automotive applications. Similarly, fences attached to the bottom and sides of the ship transom, also called interceptors, are used for ride and steering control, respectively [6]. Some numerical investigation on the interceptors are reported by Brizzolara [2] and Molini and Brizzolara [9], and this topic is still of interest with a recent experimental study published by Day and Cooper [4].

The present study is a part of ongoing work on base-ventilated hydrofoils involving numerical [10, 12] and experimental [11] investigations. Within this study a further step in the numerical modelling is presented. Ventilated cavity flow over a wall-mounted fence is investigated with a viscous approach. The effect of ventilation rate on the flow physics and hydrodynamic performance is investigated. Effects of the viscosity are evaluated through a comparison with inviscid potential flow data, obtained using a numerical boundary element method [12].

A sketch of the ventilated cavity flow over a wall mounted fence investigated is shown in figure 1. The fence, of height h, is immersed within the wall boundary layer of thickness δ, where U is 99% of the freestream velocity, U_∞. To ventilate the flow air is supplied to the wake region through the downstream face of the fence. Cavity detachment is from the fence tip and a typical re-entrant jet closure regime is illustrated. The resulting pressure distribution is indicated on the wall upstream of the fence.

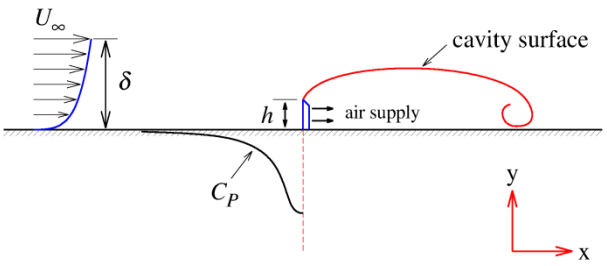

Figure 1: Sketch of a wall mounted fence immersed within the boundary layer with a ventilated cavity detaching from the sharp outer edge. Gas is supplied from the downstream face of the fence. The pressure distribution on the upstream wall is shown. The origin of the coordinate system is at the fence/wall junction.

The main dimensionless parameter governing a ventilated cavity flow is the cavitation number, $\sigma_c = (p_\infty - p_c)/0.5\rho U_\infty^2$, where p_c is the pressure inside the cavity, p_∞ is the reference freestream pressure, ρ is the liquid density and U_∞ is the reference freestream velocity. In the case of ventilated cavities, for constant free stream conditions, σ_c is determined by the air flow rate which is characterized by a volumetric flow coefficient $C_{Qv}=Q_m/\rho_{air}U_\infty S$, where Q_m is the mass flow of the supplied air, ρ_{air} is the air density and S is the surface area of the fence. A Reynolds number based on fence height, $Re_h=U_\infty h/\nu$, where ν is the kinematic viscosity, is also applicable.

Modelling

The commercial Computational Fluid Dynamics software, CD Adapco STAR-CCM+, was used for the present study. For later comparison with experimental results a rectangular computational domain was created to represent the University of Tasmania cavitation tunnel test section. The domain height was set at 60h and a fence, modelled as 10 mm high and 0.1 mm thick, was attached to the test section floor. The domain inlet and outlet were positioned sufficiently away from the fence to avoid their influence on the flow, located at 500h and 1000h respectively. For the spatial discretization, a structured hexahedral mesh with prism layer cells in the boundary layer region was used. To resolve the flow a first order implicit unsteady finite volume method was employed. Water was defined with constant density and air as an ideal compressible gas. The interface between the phases was tracked using a VOF method based on the volume fraction equation. Surface tension and gravity effects were included in the model. Gravitational acceleration was directed upwards to enable comparison with the future experimental data where the fence will be located on the test section ceiling. For the consideration of viscous effects a RANS approach with the SST (Menter) k-ω turbulence model was used.

Water enters the domain through the constant velocity inlet, with the velocity set to 10 m/s (Re_h=1×10^5) for all cases. The flow rate of injected air was varied between 0.01 kg/s and 0.09 kg/s (giving $0.084 < C_{Qv} < 0.751$). The domain outlet was defined as a constant pressure outlet, set to 50 kPa for all cases. An unperturbed boundary layer thickness at the fence position ($x = 0$) of $\delta/h = 2$ was achieved by setting the length of the free slip boundary condition on the wall upstream of the fence. The reference pressure used was defined as the minimum pressure on the wall upstream of the fence. The reference freestream velocity was chosen as the value at the vertical centreline 100h upstream of the fence.

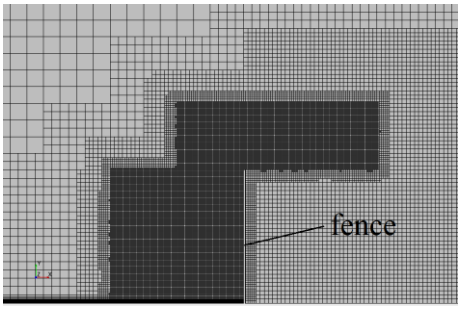

Figure 2: Local refinement of the mesh in front of the fence and in the cavity region. The prism layer on the upstream wall is also shown

A convergence analysis was done for both temporal and spatial discretization. Time steps ranging between 0.5 and 2 ms were analysed and a time step of 1 ms gave results within 1% of the independent solution. Spatial convergence was analysed with the number of cells varying between about 0.2 and 4×10^6. It was found that a mesh consisting of just over 1.8×10^6 cells gave results within 1% of the grid independent solution. Prism layer parameters are chosen to achieve y^+<1 for the wall with the fence attached and $y^+ \approx 30$ for the wall without the fence. Mesh refinement is used in the region where the cavity is expected with additional refinement upstream of the fence to resolve the separation bubble. Computational time needed to obtain a solution, using 12 cores on a multinode cluster, varied between about 20 to 30 hours. This was mainly dependent on the time needed for a cavity to fully develop, i.e. the length of the resulting cavity which was a function of the ventilation rate.

Results and Discussion

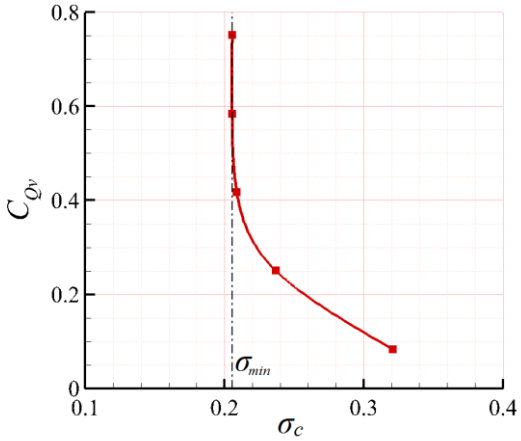

Figure 3: Relation between cavitation number, σ_c, and volumetric flowrate coefficient, C_{Qv}, for δ/h=2.

The dependence of σ_c on C_{Qv} is shown in figure 3. On the left hand side of the curve a vertical asymptote is present representing a minimum σ_c value achievable under the prescribed geometric and flow conditions. At $\sigma_c = \sigma_{min,}$ the flow is said to be 'blocked' [1], analogous to the choked condition of compressible flow though valves and orifices, and is a function of the degree of confinement of the flow domain. The extent of the confinement/blockage is expressed in terms of the ratio of the domain height, H, and the fence height, which for the present study was a value of H/h=60. Significantly lower values of σ_{min} are achieved for the cases with a boundary layer present compared to the potential flow case with the same blockage conditions, with the values of σ_{min} being 0.2054 and 0.2957, respectively.

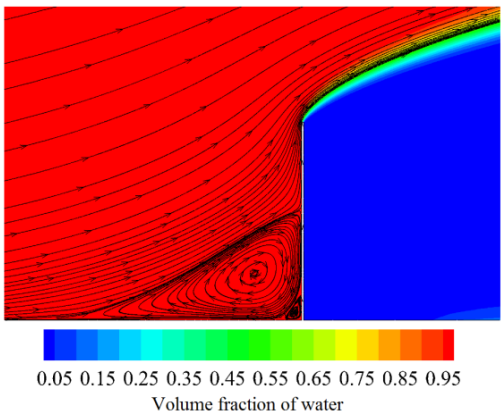

Figure 4: Streamlines depicting flow topology upstream of the fence (σ_c = 0.2368, δ/h = 2) showing the upstream separation zone. The cavity surface, including the detachment from the fence tip, is also shown as contours of volume fraction.

The flow topology upstream of the fence is shown in figure 4. A separation bubble is present as would be expected for a viscous flow over a forward-facing step. It can be seen that under the main vortex, at the fence/wall junction, a secondary counter-rotating vortex is present. It was found that the size of the separation zone doesn't vary significantly with respect to σ_c. Stagnation points were located at $x = -1.73h$ on the wall and $y = 0.57h$ on the fence for the main vortex, and $x = -0.1h$ on the wall and $y = 0.16h$ on the fence for the secondary vortex. The cavity detaches from the fence and the gas-liquid interface is

represented as a smeared zone in contrast with the defined free surface present in the potential flow formulation.

Closure of a ventilated cavity on the downstream wall exhibits re-entrant jet behaviour. Depending on the flow conditions gas discharge from the cavity closure may be continuous or as large bubbly structures detaching from the cavity periodically. The latter regime is described as a pulsating cavity [7]. A typical example of the closure region of a pulsating cavity is shown in figure 5. The streamlines show that a bubble is close to detachment with the formation of a new bubble upstream. A re-entrant jet flow can be observed diverting liquid upstream along the wall into the cavity. For short cavities the re-entrant jet transports liquid almost up to the fence, with most of the cavity consisting of a liquid/gas mixture. For the longer cavities, the re-entrant jet only extends a limited extent leaving the upstream cavity region completely filled with air only. When σ_c reaches σ_m, the cavity length becomes 'infinite' extending to the domain outlet. With a further increase in C_{Qv} the cavity geometry remains unchanged, but the computational time needed for the cavity to reach the domain outlet is shortened.

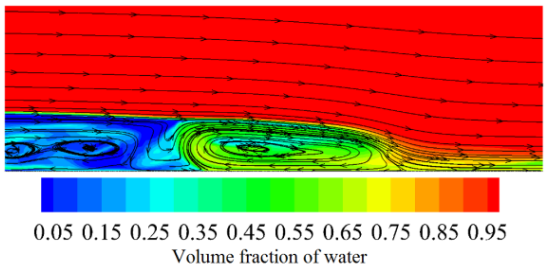

Figure 5: Closure region of the cavity represented with volume fraction contours (σ_c = 0.2368, δ/h = 2). Streamlines show a bubble about to detach and a new bubble starting to form in the cavity upstream.

As the closure region consists of a mixed phase, volume fraction contours could not be used to determine cavity length. Instead, the location of the stagnation point downstream of the cavity, where the flow divides into the re-entrant jet and wake region, is used to determine cavity length. The stagnation point manifests as a peak in the wall pressure distribution downstream of the fence. For the pulsating regime, several peaks were present due to the bubbles already detached from the cavity and the one associated with the main cavity closure was used to determine cavity length. Time averaging was necessary to establish a mean value of the length for the pulsating cavities. The cavity oscillations were typically in the order of 20% of the mean length. The dependence of cavity length on cavitation number is shown in figure 6. The viscous (δ/h=2) and potential flow data exhibit similar behaviour, with cavities growing infinitely when σ_m is reached. In an unbounded flow the cavity length behaves in accordance with a power law with respect to σ_c ([7], [12]). The effect of the boundary layer can be observed as a left hand translation of the potential flow curve, i.e. same cavity length is achieved for a lower cavitation number.

The influence of the ventilation rate on the wall pressure distribution upstream of the fence, and ultimately on the lift, is of interest. Figure 7 shows a double log plot of the pressure distribution (with $C_p = (p - p_\infty)/0.5\rho U_\infty^2$), along the upstream wall. The wall pressure distributions for all cases display an exponential like reduction with upstream distance. A C_p of 0.001 was chosen as a level to determine a length of influence of the fence. It was found that with an increase in C_{Qv}, the length of influence increased, but the rate of increase reduces to zero as $\sigma_c \rightarrow \sigma_m$. The length of influence increases by about 7% over the C_{Qv} range investigated up to maximum of about 80h (see lower inset in figure 7).

Also of interest is the maximum value of the pressure coefficient, $C_{p\,max}$, for x/h=0. $C_{p\,max}$ behaves similarly to the length of influence with increasing C_{Qv} reaching an asymptotic value with $\sigma_c \rightarrow \sigma_m$. Overall increase in $C_{p\,max}$ is about 4%, with the maximum value just over 0.4 (see upper inset in figure 7). The boundary layer effect lowers $C_{p\,max}$ by approximately 60% compared with the potential flow result (where $C_{p\,max}$=1). This is due to the fence immersion within the boundary layer resulting in a locally lower velocity at the fence height compared with the uniform velocity profile in the potential flow solution.

For the range of ventilation rates investigated the hydrodynamic parameters (lift, drag and lift to drag ratio) have a power law dependence on σ_c as shown in figure 8. Lift and drag are non-dimensionalised using the fence height giving, $C_L = L/0.5\rho U_\infty^2 h$ and $C_D = D/0.5\rho U_\infty^2 h$. Lift was calculated as the integral of the pressure distribution on the wall upstream of the fence over a

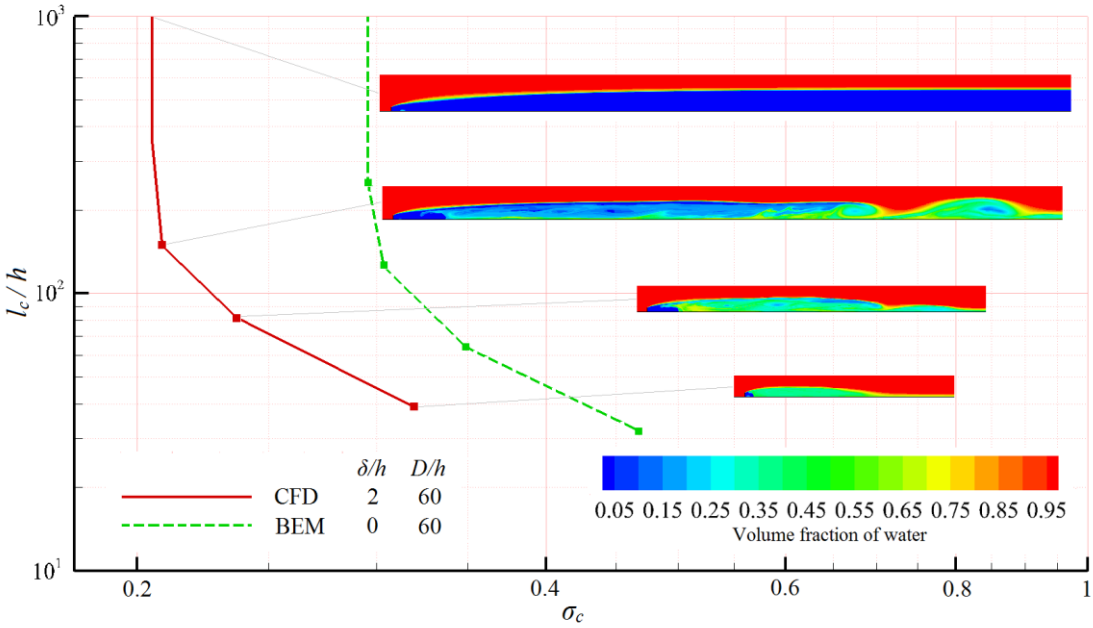

Figure 6: Cavity length (l_c/h) as a function of cavitation number (σ_c) for the viscous (δ/h=2) and potential flow cases with the same blocakge ratio, H/h=60. Cavity topology for all viscous cases is shown using contours of volume fraction.

length of 100h. As discussed above this distance is sufficient to determine the lift. The lift added between 60h and 100h is limited to below 0.5% of the total. Increase in the ventilation rate leads to increase in the lift, which can be attributed to the higher value of the $C_{p\,max}$ and greater length of influence of the upstream wall pressure. Lift increased 18% over the range of ventilation rates investigated. Drag was calculated from the integral of the pressure distribution over the front and back faces of the fence. Drag decreases with decrease in σ_c, with the difference between highest and lowest values being about 15%. This can be attributed to the effect of cavity pressure on the back face of the fence as the ventilation rate increases. Both of these aspects contribute positively to an increase in the lift to drag ratio with increasing ventilation rate, reaching the maximum value for $\sigma_c = \sigma_m$. The lift to drag ratio increases by about 30% over the range of ventilation rates investigated.

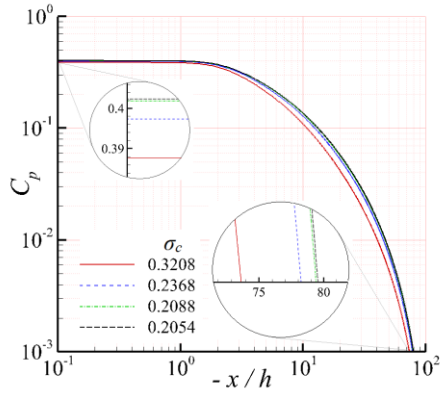

Figure 7: Wall pressure distribution upstream of the fence (with δ/h=2).

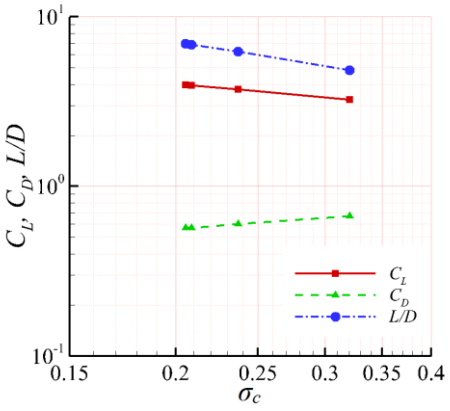

Figure 8: Dependence of hydrodynamic parameters C_L, C_D and L/D on σ_c

Conclusions

Ventilated cavity flow over a 2-D wall mounted fence was investigated numerically using a viscous approach with some comparison made with potential flow results from a boundary element method analysis. Dependence of the cavitation number on volumetric flow rate coefficient is established. Cavity flow topology was determined, with a separation zone in front of the fence and a re-entrant jet closure captured. Cavity length exhibits similar general behaviour with the respect to cavitation number for both the viscous and potential analyses, with the same cavity length occurring at a lower cavitation number with a boundary layer present. Upstream wall pressure data shows that maximum pressure (i.e. stagnation at the fence/wall junction) and the length of wall influenced by the presence of the fence varies with respect to C_{Qv}. A lift (spanwise) force results from the imposed pressure distribution due to the addition of a fence which increases with ventilation rate. The drag (streamwise) force on the fence also reduces as ventilation is increased resulting in an increase in hydrodynamic efficiency

Further numerical investigation into the effects of the overlying boundary layer and flow confinement on cavity geometry and hydrodynamic performance is required. A companion experimental investigation is also planned for comparison with the numerical study.

References

[1] Brennen, C. E., Cavitation and Bubble Dynamics, New York, Oxford University Press, 1995.

[2] Brizzolara, S., Hydrodynamic analysis of interceptors with CFD methods, in *Seventh International Conference on Fast Sea Transportation - FAST 2003*, Naples, Italy, 2003, 49-56.

[3] Ceccio, S. L., Friction drag reduction of external flows with bubble and gas injection, *Annu. Rev. Fluid Mech.* **42**, 2010, 183-203.

[4] Day, A. H. & Cooper, C., An experimental study of interceptors for drag reduction on high-performance sailing yachts, Ocean Engineering **38**(8–9), 2011, 983-994.

[5] Elms, A. R., Improved Hydrofoil Device, International Patent Number WO 99/57007, W. I. P. Organization, 1999.

[6] Faltinsen, O. M., Hydrodynamics of high speed vehicles, Cambridge, England, Cambridge University Press, 2005.

[7] Franc, J. P. & Michel, J. M., Fundamentals of Cavitation, Dordrecht, Kluwer Academic Publishers, 2004.

[8] Matveev, K. I., Burnett, T. J. & Ockfen, A. E., Study of air-ventilated cavity under model hull on water surface, Ocean Engineering **36**(12–13), 2009, 930-940.

[9] Molini, A. & Brizzolara S., Hydrodynamics of interceptors: a fundamental study, in *International Conference on Maritime Research and Transportation ICMRT 2005*, Ischia, Italy, 2005.

[10] Pearce, B. W., Brandner, P. A. & Binns, J. R., A numerical investigation of the viscous 2-D cavitating flow over a wall-mounted fence, in *17th Australasian Fluid Mechanics Conference*, Auckland, New Zealand, 2010.

[11] Pearce, B. W. & Brandner, P. A., Experimental investigation of a base-ventilated supercavitating foil with interceptor, in *8th International Symposium on Cavitation, Cav 2012*, Singapore, 2012.

[12] Pearce, B. & Brandner, P., Inviscid cavity flow over a wall-mounted fence, Ocean Engineering **80**, 2014, 13-24.

[13] Semenenko, V. N., Artificial Supercavitation, Physics and Calculation, Lecture Notes from the RTO AVT/I Special Course on Supercavitating Flows, von Karman Institute for Fluid Dynamics, Rhode Saint Genese, Belgium, 2001.

[14] Storms, B. L. & Jang, C. S., Lift enhancement of an airfoil using a Gurney flap and vortex generators, Journal of Aircraft **31**(3), 1994, 542-547.